Blending with a phthalocyanine leads to improved P3HT donor layers for OPVs

Diego Fernando Silva Sousa, Marta Elisa Rosso Dotto, Juliana Eccher, Harald Bock, Ivan Bechtold

Blending with a phthalocyanine leads to improved P3HT donor layers for OPVs

Diego Fernando Silva Sousa[a], Marta Elisa Rosso Dotto[a], Juliana Eccher[a], Harald Bock[b], Ivan H. Bechtold[a,*]

[a] Departamento de Física, Universidade Federal de Santa Catarina, 88040900, Florianópolis, SC, Brazil
[b] Centre de Recherche Paul-Pascal, CNRS - University of Bordeaux, 33600, Pessac, France

ARTICLE INFO

Keywords:
OPV
Donor blend
Phthalocyanine
Discotic liquid crystal
P3HT
Charge transport

ABSTRACT

Ternary blended solar cells have been intensively studied in recent years, where the addition of a second donor material in the active layer tends to increase the current density through improved photon absorption along with improving the charge transport properties and the inhibition of charge recombination processes. Here, we investigated a donor layer composed of a liquid crystalline cobalt phthalocyanine (CoPc) and poly(3-hexylthiophene-2,5-diyl) – P3HT. The CoPc presents a complementary absorption spectrum in the near infrared region and compact anisotropic molecular arrangement to promote efficient charge migration. The energy levels of CoPc are properly located between the corresponding levels of P3HT and PCBM, forming an energy cascade alignment. The P3HT/CoPc blend showed improved photophysical and electrical response depending on the CoPc concentration and thermal annealing. We demonstrated that molecular order, morphology and energetic barrier at cluster interfaces are competing effects and need to be taken into account to optimize charge transport.

1. Introduction

Research on sustainable and clean energy sources is continuously under investigation [1]. Photovoltaic devices based on organic materials are a real alternative that has attracted interest from the scientific community in the last two decades, considering advantages such as easier solution processability, lower production cost, possibility of malleability and transparency, large area devices and less environmental impact [1,2].

However, the performance of organic photovoltaic (OPV) devices is affected by the limited absorption of the sunlight spectrum and the low charge carrier mobility of the active layer, which result in low current density and consequently poor photovoltaic performance. Recently, using the concept of ternary blends, electron donating materials with complementary energy bands were used to increase light absorption and efficient devices were obtained [3–6]. Polymers, small molecules, fullerene derivatives, dyes, graphene-based materials, nanocrystals, non-fullerene n-type organic semiconductors and liquid crystals are generally used to complement the photophysical properties of the active layer [7]. Recently, non-fullerene based OPVs have demonstrated power conversion efficiency higher than 15 % in a single junction architecture [8].

Discotic liquid crystals (DCLs) have rigid cores with a conjugated electronic system surrounded by aliphatic flexible chains. The conjugated π-electronic system favors molecular stacking in a columnar structure that is responsible for charge conduction, preferably by hopping processes, while the aliphatic chains act as insulating sheath. These systems present anisotropic electronic conductivity along the columnar axis, several orders of magnitude higher than in the perpendicular direction [9–12]. The columns exhibit high exciton diffusion lengths and charge carrier mobility that can reach the order of 1 cm^2/V.s [12,13]. Therefore, DLCs attracted attention due to their self-organizing and photophysical properties, being used as additives in OPVs [6,13–16], organic light-emitting diodes (OLEDs) [17,18] and organic field effect transistors (OFETs) [19–21].

Cao et al. obtained an efficiency of 11.40 % by incorporating the liquid crystal benzodithiophene terthiophene rhodanine in the state-of-the-art mixture PTB7-Th:PC71BM [6], which induced a more efficient phase separation and better charge transport, resulting in an efficiency increase of 25 % in comparison to the binary system. Ozaki et al. studied the addition of a metal-free phthalocyanine liquid crystal to the conventional P3HT:PCBM blend, resulting in a 2.3 %–3.0 % gain in efficiency. The phthalocyanine contributed to light absorption between 650–800 nm and to the molecular ordering of the blend, increasing the

current density from 8.6 to 12.6 mA.cm^{-2} [13]. Recently, Fujii et al. obtained a high hole mobility, reaching 1.45 cm^2/V.s, for phthalocyanine liquid crystals, and OPVs using PCBM as acceptor displayed an efficiency of 5.3 % [13]. Many other works have also improved the efficiency with the use or addition of a liquid crystal in the active layer [12,16,22].

In this work, a cobalt phthalocyanine (CoPc) was blended together with P3HT to act as electron donor layer in OPVs. Different from the literature, this CoPc adopts a columnar rectangular plastic packing at room temperature after heating until 160 °C, known as the compactest molecular arrangement for DCLs, prone to improve charge transport. The photophysical, structural, morphological and electrical properties were studied under ambient conditions and after thermal annealing at 160 °C to investigate the contribution of molecular ordering on these properties. HOMO and LUMO of the CoPc are located between the corresponding levels of the electron donor and acceptor materials used in OPVs, forming a cascade alignment, which favors energy and charge transfer between the acting materials. The CoPc contributed to widen the sunlight absorption spectrum and the charge carrier mobility of the blend was improved by two orders of magnitude.

2. Experimental

The synthesis of the CoPc, cobalt 1,8,15,22-tetra-(2-butyloctyloxy)-phthalocyaninate, has been published elsewhere [23]. The compound is crystalline at room temperature, but presents a columnar rectangular mesophase between 54 and 294 °C on heating, which adopts a rectangular columnar plastic crystalline phase below 42 °C after cooling. The regioregular polymer P3HT (poly(3-hexylthiophene-2,5-diyl)) was purchased from Sigma Aldrich. The molecular structures of CoPc and P3HT are shown in Fig. 1.

The liquid crystalline behavior of the CoPc was studied with an Olympus BX50 polarizing optical microscope (POM) in transmission mode, equipped with a Mettler Toledo FP-82 hot stage for temperature control. The images were captured with a CCD camera coupled with the microscope.

X-ray diffraction (XRD) experiments were done with a CuKα radiation X'Pert PRO (PANalytical) diffractometer (λ = 1.5418 Å) equipped with an X'Celerator detector. The films were deposited by spin-coating onto glass substrates and measured before and after annealing. The diffraction radiation was collected in continuous mode from 2° to 9° (2θ angle).

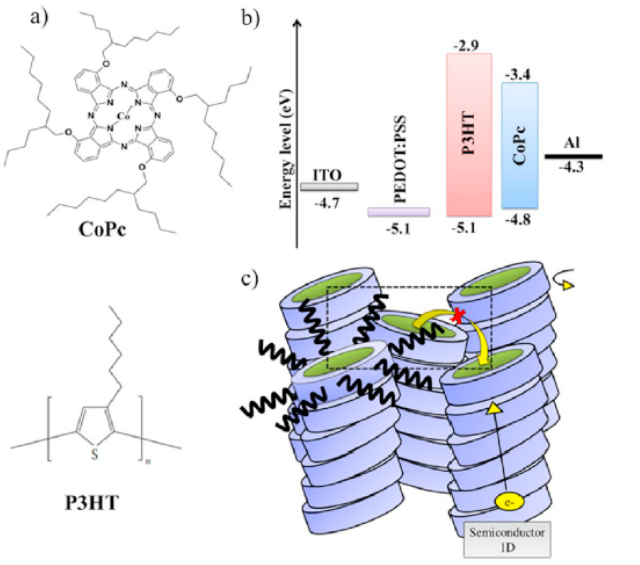

Fig. 1. (a) Molecular structures of CoPc and P3HT. (b) Energy level diagram of the device and (c) Representation of the CoPc rectangular columnar mesophase.

UV–vis absorption in ortho-dichlorobenzene (ODCB) solution and spin-coated films was collected with an Ocean Optics USB400 spectrophotometer. Measurements in solution were performed at initial concentrations of 4.9 × 10^{-3} mg/mL.

Diodes were produced by solution processing of the CoPc and P3HT individually and blended with CoPc weight proportions of 10 %, 15 %, 25 %, 50 % and 75 %. Indium tin oxide (ITO) coated glass plates with a sheet resistance of 15 Ω/□ were used as conductive substrates. A thin layer of PEDOT:PSS [poly(3,4-ethylenedioxythiophene) poly(styrenesulfonate)] was deposited by spin coating at 500 for 2 s, 1500 rpm during 30 s and 3000 rpm for 30 s followed by annealing at 120 °C for 10 min. The organic semi-conductor layers were deposited by spin-coating at 1000 rpm during 60 s. The CoPc was solubilized with chloroform (Chl), while the P3HT was solubilized with ODCB, both at 10 mg/mL concentration. In the case of the mixed devices, the films were produced with mixed solvents, Chl and ODCB, keeping the same weight proportion as of the compounds. The mixed solutions were stirred during 24 h at room temperature prior to deposition. Finally, the Al electrode (100 nm) was deposited onto the top of active layer at a rate of 1 Å/s under a vacuum pressure of 10^{-7} mbar. The active area of the diodes was 6 mm^2. J/V curves were measured under ambient conditions at room temperature (25 °C) using a Keithley source measuring unit (Series 2400).

The thickness and roughness of the spin-coated films were probed by atomic force microscopy (AFM), using a Nanosurf EasyScan 2 apparatus in tapping mode with a scanning rate of 1.0 Hz covering a lateral size of 10 μm × 10 μm with resolution of (512 × 512) pixels. Thermal annealing at 160 °C during 10 min was performed on the films using a hot stage.

3. Results

The CoPc was first analysed by polarizing optical microscopy, where a dendritic texture typical of columnar organization is present at room temperature, shown in Fig. S1 of the Supporting Information. This indicates that the columnar molecular organization is preserved in ambient conditions and at room temperature.

Absorption experiments in solution and in film are shown in Fig. 2. In solution, the 50 % mixture yields the composed spectrum of the individual absorption bands, providing a wider absorption range (Fig. 2(a)). The peripheral peaks, which are characteristic of phthalocyanines [9,12–15,24,25], are due to the absorption of CoPc. The absorption band above 600 nm is in the region where the sun has the maximum photon emission to increase charge generation [26]. The broad central band represents the absorption spectrum of P3HT [27–29]. The solution absorption spectra of the mixtures in different proportions preserve the vibrational characteristics of both materials. The absorption peaks are due to $\pi-\pi^*$ transitions [14].

Fig. 2(b) shows the absorption spectra of CoPc and P3HT films, with and without thermal annealing. The broadening of the spectra of the films compared to the solutions is characteristic of molecular aggregation with stronger intermolecular interactions in solid state, where $\pi-\pi$ type interactions become more intense. The frontier orbitals of CoPc lead to an energy level cascade within the P3HT:PCBM system, which favors exciton dissociation and charge transfer [4,14,30,31]. The P3HT film exhibited an absorption band from 370 to 670 nm, representing characteristic transitions related to interchain exciton dislocation [32]. The shoulder at approximately 600 nm is attributed to the ordering of the P3HT film [28].

The thermal annealing induces rearrangement of the aliphatic chains, which affects the crystallinity of the compounds and increases the $\pi-\pi$ interactions [11,12,29]. This leads to an increase in the absorption spectrum of both materials, resulting in an improvement of the optical, structural and charge transport properties [33,34].

The 1:1 CoPc:P3HT blend shows a remarkably continuous absorption between 300 nm and 750 nm, which is desired for sunlight energy

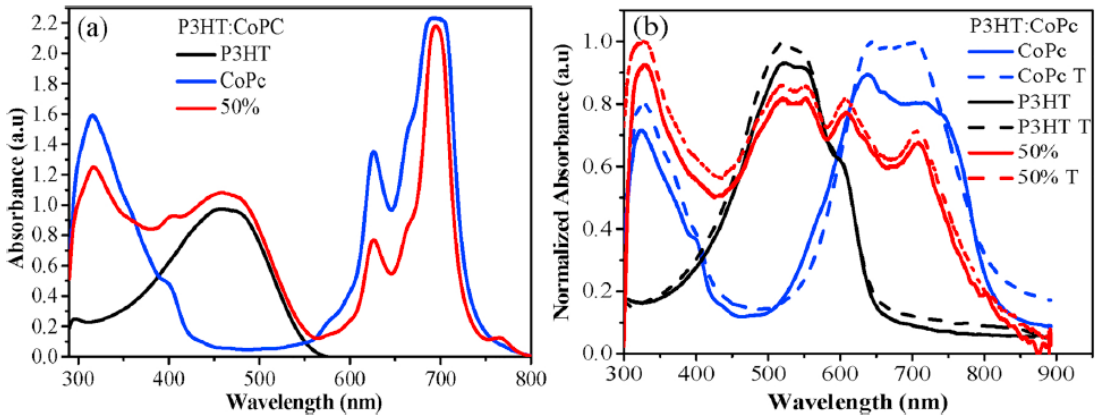

Fig. 2. Absorption spectrum of the CoPc and P3HT and of their 1:1 mixture in ODBC solution (a) and in spin-coated film (b). Dashed lines correspond to thermally annealed (T) films (160 °C, during 10 min).

conversion. Absorption spectra of films with other blend ratios are shown in Fig. S2 of the Supporting Information.

X-ray diffraction patterns for P3HT, CoPc and P3HT:CoPc films at 10 %, 15 %, 25 %, 50 %, and 75 % of CoPc before and after thermal annealing are shown in Fig. 3(a) and (b). The CoPc diffractograms present two intense and narrow diffraction peaks at $2\theta = 4.58°$ ($d_{11} = 19.3$ Å) and 5.17° ($d_{20} = 17.1$ Å), yielding the columnar rectangular lattice parameters $a = 23.4$ Å and $b = 34.2$ Å [23]. The P3HT film exhibited a weak diffraction peak around $2\theta = 5.38°$, corresponding to the interchain distance of 16.7 Å [14,22]. The P3HT doping with CoPc not only increases the XRD peak intensity of CoPc, but also the P3HT peak (Fig. 3b), both coexisting within the bulk heterojunction, similar to other works [14,25]. This improvement in the blend crystallinity can be attributed to the self-ordering of the liquid crystal molecules [12,13,35]. The π-stacking interactions of CoPc contribute to improve the packing order of P3HT chains. Thermal annealing enhances the π-stacking interactions, increasing the intensity of the diffraction peaks.

The grain size of the nanocrystalline structure (D) was calculated using the Scherrer equation: ($D = \frac{0.94\lambda}{\beta\cos\theta}$) [36]. Where β is the full-width at the half-maximum of the XRD peak, obtained by fitting the peak at 2θ angle with a Gaussian function. The β and D values are shown in Table 1. For the pure films, CoPc ($2\theta = 5.17°$) and P3HT ($2\theta = 5.38°$) the tendency of β reduction and increase of D was observed after thermal annealing, as expected due to improvement of the film crystallinity. For the blended films, the thermal annealing also improved film crystallinity. Moreover, for the annealed films, the effect of P3HT doping with CoPc (10 %–75 %) on the CoPc peak shows pronounced reduction of β (0.68 – 0.10) and consequent increase of D (12.22–83.90). The effect of doping on the P3HT peak was noticed only for high CoPc concentrations (50 % and 75 %) and specially after annealing. These results suggest that CoPc serves as a nucleating agent to facilitate the crystallization of P3HT [37,38].

Fig. 4 shows the AFM morphologies of the P3HT:CoPc blends with 10 %, 25 % and 75 % of CoPc in the device structure for electrical characterization, before and after thermal annealing. The root-mean-square roughness (R_{rms}) values are displayed in Table 2. The thickness found for the blends was 60 nm and there were no significant changes after thermal annealing.

In OPVs containing P3HT:PCBM typically o-dichlorobenzene or chlorobenzene solvents are used, however these solvents were inappropriate for CoPc due to its low substrate wettability. The difficulty of film deposition with these solvents was reported previously with liquid crystalline phthalocyanines [14,25]. Therefore, mixed solvents containing o-dichlorobenzene and chloroform were used to produce the blended films, which presented surfaces with homogeneous morphology with very uniform domains and structures. The R_{rms} values in the range of 4.6 nm are appropriate for efficient exciton dissociation and charge transport in devices. An exception is the 75 % CoPc blend, where the thermal annealing seems to promote excessive molecular aggregation and phase separation, resulting in an R_{rms} of 12.9 nm.

Diodes with ITO/PEDOT:PSS/**P3HT:CoPc**/Al were prepared in order to determine the charge carrier mobility of the active layer, consisting of pure P3HT, pure CoPc and blends with 10 %, 25 %, 50 % and 75 % of CoPc. The effect of thermal annealing was also investigated. The devices were prepared and measured at room

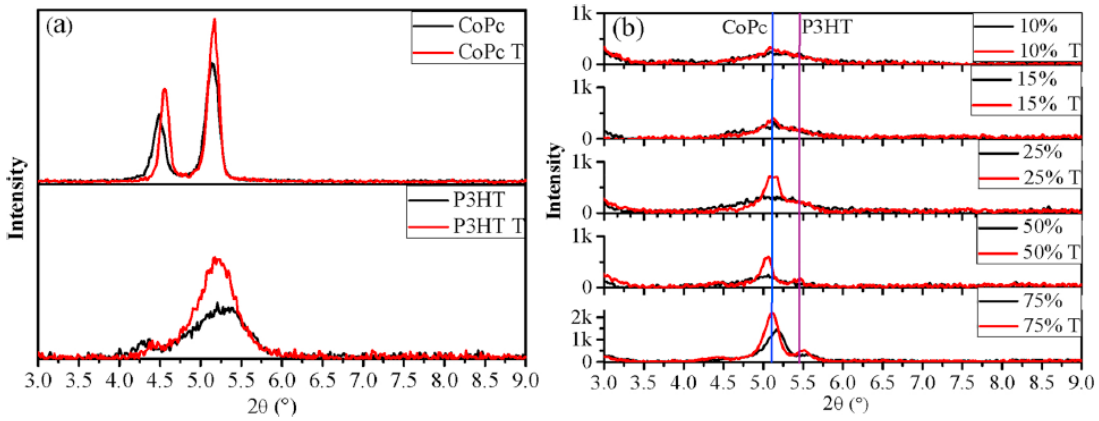

Fig. 3. X-ray diffractograms obtained for CoPc and P3HT (a) and P3HT:CoPc blends in the proportions 10 %, 15 %, 25 %, 50 % and 75 % of CoPc (b). T indicates thermal annealing of 160 °C during 10 min (red curves).

Table 1
Full-width at the half-maximum of the XRD peak (β) and grain size of the nanocrystalline structure (D) calculated using the Scherrer equation.

Films	2θ = 5.17° (CoPc peak)				2θ = 5.38°(P3HT peak)			
	β (°2θ)	D (nm)	$\beta\ (°2\theta)_T$	$D\ (nm)_T$	β (°2θ)	D (nm)	$\beta\ (°2\theta)_T$	$D\ (nm)_T$
P3HT	–	–	–	–	0.71	11.7	0.56	14.48
10 %	0.89	9.34	0.68	12.22	–	–	–	–
15 %	0.97	8.57	0.59	14.08	–	–	–	–
25 %	0.97	8.57	0.31	26.81	–	–	0.26	31.96
50 %	0.66	12.59	0.17	48.88	–	–	0.31	26.81
75 %	0.32	25.97	0.10	83.90	0.33	25.10	0.21	39.57
CoPc	0.19	43.73	0.15	52.59	–	–	–	–

T indicates results after thermal annealing.

temperature and ambient atmosphere and protected from light.

Fig. 5 shows the current density *versus* voltage plot for the 25 % CoPc blend before (a) and after (b) thermal annealing (see Fig. S3 of the Supporting Information for other concentrations). The log-log plots clearly show the ohmic regime at lower voltages and the space-charge-limited-current (SCLC) regime beyond the threshold voltage (V_Ω) of about 2 V in both cases. The log(J) × V plots (inset in (a) and (b)) show a modest rectification, less than two orders of magnitude, representing a weak diode-like behavior. However, the rectification became one order of magnitude higher after thermal annealing, indicating that charge transport was improved by this process.

The height of the energy barrier for charge injection through the contacts is one of the factors limiting charge transport in organic semiconductors. The CoPc and P3HT energy levels, as well as the electrode work functions, are shown in Fig. 1(b). The PEDOT:PSS energy level –5.1 eV is very close to the HOMO energy levels of P3HT and CoPc, which favors hole injection in both materials. However, the high electron injection barrier at the Al electrode may cause asymmetric injection of holes and electrons inside the active layer.

The ohmic regime is characterized by $J \propto V^n$, with $n = 1$. To extract the charge carrier mobility, the Mott-Gurney law is generally used, with $J \propto V^2$, that represents a trap-free SCLC regime. However, this was not observed in the results presented here ($J \propto V^n$, with $n > 2$). To find the dependence of the charge mobility with the applied electric field, at a constant temperature, we used a theoretical model developed previously in our group considering a trap-limited SCLC regime [32]. In this model the charge transport is described by the hopping mechanism of Bässler [39], $\mu\ (E) = \mu_0(T)e^{\gamma\sqrt{E}}$, where μ_0 is defined as the mobility at zero field and γ resembles a Poole-Frenkel coefficient which accounts for the asymmetry of the potential wells generated by the electric field E. The μ_0 and γ parameters can be obtained directly by fitting the theoretical log(J) × log(V) curves to the experimental ones in the SCLC regime.

Table 2
R_{rms} values of the films (± 0.2 nm). Percentages indicate the amount of the CoPc in P3HT.

Films	10 %	25 %	75 %
Before T	4.8	4.6	4.4
After T	4.7	4.2	12.9

The slope coefficients of the log-log curves in the SCLC regime of Fig. 5(a) and (b) were $n = 7.3$ and 6.1 for 25 % of CoPc, before and after annealing, respectively. The colored lines in the SCLC regions

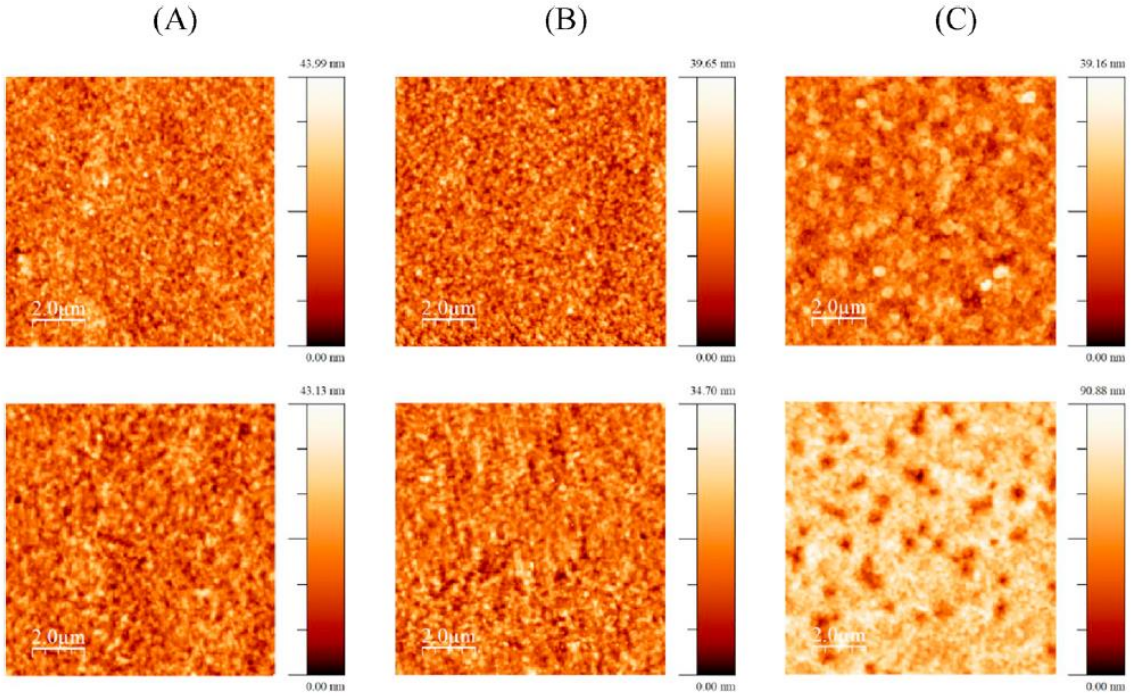

Fig. 4. 10 µm × 10 µm AFM images. Columns A, B and C represent 10 %, 25 % and 75 % of CoPc in P3HT, respectively. First row: as-prepared; second row: after thermal annealing at 160 °C during 10 min.

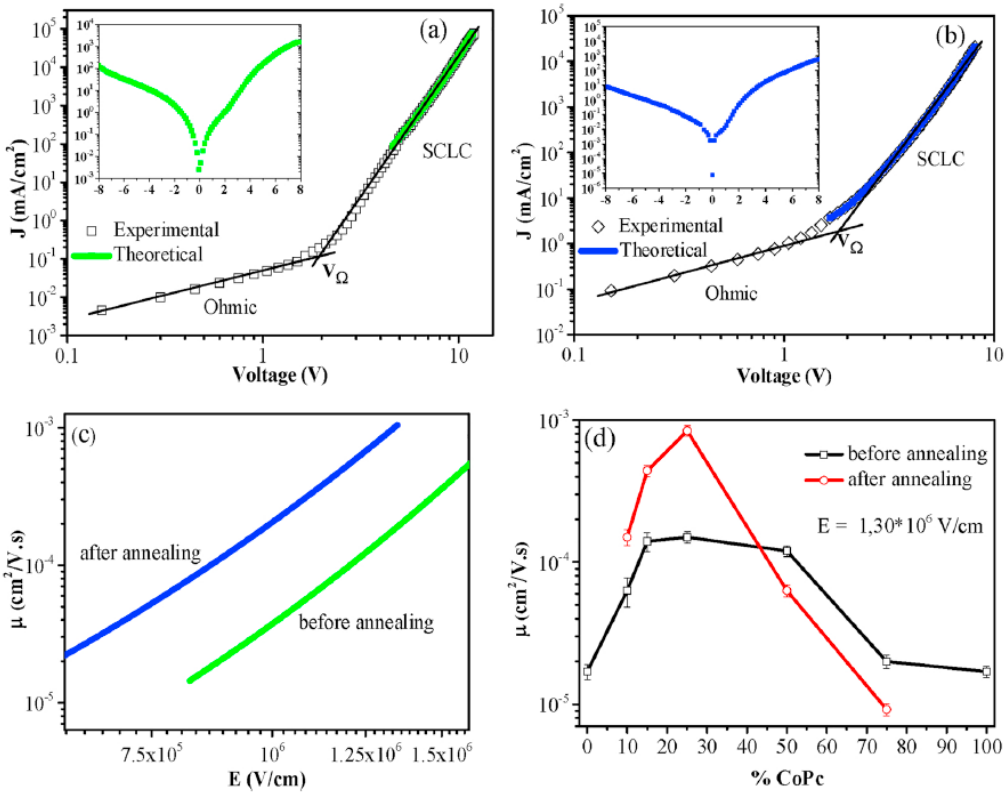

Fig. 5. Log-log plot of current density (J) *versus* voltage (V) for the blend with 25 % CoPc before (a) and after (b) thermal annealing of 160 °C during 10 min; insets: the respective log(J) × V plots. The colored lines in (a) and (b) indicate the theoretical modeling, and (c) illustrates the respective mobilities (μ) as a function of the applied electric field (E). (d) Mobilities for a given electric field as a function of the CoPc percentage, with and without annealing.

represent the fitting. The mobility as a function of the electric field (Fig. 5c) can be simulated using the Bässler equation with the obtained μ_0 and γ parameters, where the mobility is improved by about one order of magnitude by thermal annealing.

Fig. 5(d) shows the charge carrier mobilities of the devices of different blend proportions with and without thermal annealing. The values were compared for the same internal electric field of 1.3×10^6 V/cm. The neat CoPc and P3HT films presented a similar mobility around 1.5×10^{-5} m^2/V.s. The introduction of CoPc inside P3HT improved the mobility, which can be attributed to an increase of the film crystallinity, as suggested by the X-ray studies. Moreover, the γ values obtained from fitting are higher for the blended films (see Table S1 in the Supporting information), which indicates that transport *via* hopping was facilitated.

The thermal annealing was efficient to increase the mobility for 10 %, 15 % and 25 % of CoPc, indicating a rarefication or shallowing of trap sites, which limit charge transport. The annealed 25 % CoPc device presented a mobility of 8.5×10^{-4} cm^2/V.s, the best result among all devices, representing an increase of approximately two orders of magnitude compared to the CoPc and P3HT net films. On the other hand, for 50 % and 75 % of CoPc the mobility was reduced after thermal annealing. The AFM measurements showed an increase in the amount of clusters, peaks and defects for 50 % and 75 % of CoPc, which can act as new trapping sites. For 75 %, R_{rms} rised from 4.4 nm to 12.9 nm by annealing [36,37]. The effect of thermal annealing on the charge transport properties of pure P3HT has already been investigated by others, where an increase of less than one order of magnitude of the charge carrier mobility was reported [40,41], which is below the effect observed by us on 10 % CoPc blending.

Thus, the charge transport properties of the blends are closely dependent on the molecular ordering, film morphology and energetic intergranular barriers arising from molecular cluster interfaces. These are competing effects that have to be considered for device applications.

4. Conclusion

We investigated the electrical properties of a range of P3HT:CoPc blends, with 10 %, 15 %, 25 %, 50 % and 75 % of CoPc. CoPc is a high order liquid crystalline phthalocyanine that exhibits absorption in the near infrared region, complementing the absorption spectrum of P3HT. The addition of CoPc improved the charge carrier mobility. The annealed 25 % CoPc blend showed the best result, with mobility of 8.5×10^{-4} cm^2/V.s, an effective increase of approximately two orders of magnitude over the individual compounds. It was observed that the rectangular columnar structures of the CoPc molecules contributed to the crystallinity of P3HT. From the morphological parameters, the effects of the proportion of the CoPc on the blend were analyzed, as well as the effects of thermal annealing. The annealing-induced cluster formation for concentrations higher than 50 % of CoPc, led to decreased charge transport. This illustrates that molecular order, morphology and energetic barriers at cluster interfaces are competing effects and need to be taken into account to optimize the electric properties of the blend. The 3:1 P3HT:CoPc system may be a good candidate to be applied as a donor material in organic photovoltaics.

CRediT authorship contribution statement

Diego Fernando Silva Sousa: Formal analysis, Investigation. **Marta Elisa Rosso Dotto:** Supervision, Project administration, Writing - original draft. **Juliana Eccher:** Investigation, Project administration. **Harald Bock:** Formal analysis, Writing - review & editing. **Ivan H. Bechtold:** Supervision, Project administration, Writing - original draft.

Declaration of Competing Interest

Authors declare that there is no conflict of interest for publication of the manuscript.

Acknowledgments

The authors are grateful to CNPq, CAPES, FAPESC, INCT-INEO, H2020-MSCA-RISE-2017 (OCTA, #778158) and CAPES-COFECUB (# 803-14) for financial support. The XRD experiments were carried out in the Laboratório de Difração de Raios-X (LDRX-CFM/UFSC).

References

[1] S. Rafique, S.M. Abdullah, K. Sulaiman, M. Iwamoto, Fundamentals of bulk heterojunction organic solar cells: an overview of stability/degradation issues and strategies for improvement, Renew. Sustain. Energy Rev. 84 (2018) 43–53, https://doi.org/10.1016/j.rser.2017.12.008.

[2] G.A. Chamberlain, Organic solar cells: a review, Sol. Energy Mater. Sol. Cells 8 (1983) 47–83, https://doi.org/10.1016/0379-6787(83)90039-X.

[3] J. Farinhas, R. Oliveira, R. Hansson, L.K.E. Ericsson, E. Moons, J. Morgado, A. Charas, Efficient ternary organic solar cells based on immiscible blends, Org. Electron. 41 (2017) 130–136, https://doi.org/10.1016/j.orgel.2016.12.009.

[4] F. Wu, Y. Shan, R. Wang, L. Zhu, Incorporation of diketopyrrolopyrrole dye to improve photovoltaic performance of P3HT:PC 71 BM based bulk heterojunction polymer solar cells, Org. Electron. 31 (2016) 171–176, https://doi.org/10.1016/j.orgel.2016.01.028.

[5] K. Weng, C. Li, P. Bi, H.S. Ryu, Y. Guo, X. Hao, D. Zhao, W. Li, H.Y. Woo, Y. Sun, Ternary organic solar cells based on two compatible PDI-based acceptors with an enhanced power conversion efficiency, J. Mater. Chem. A 7 (2019) 3552–3557, https://doi.org/10.1039/C8TA12034J.

[6] G. Zhang, K. Zhang, Q. Yin, X.-F. Jiang, Z. Wang, J. Xin, W. Ma, H. Yan, F. Huang, Y. Cao, High-performance ternary organic solar cell enabled by a thick active layer containing a liquid crystalline small molecule donor, J. Am. Chem. Soc. 139 (2017) 2387–2395, https://doi.org/10.1021/jacs.6b11991.

[7] L. Duan, N.K. Elumalai, Y. Zhang, A. Uddin, Progress in non-fullerene acceptor based organic solar cells, Sol. Energy Mater. Sol. Cells 193 (2019) 22–65, https://doi.org/10.1016/j.solmat.2018.12.033.

[8] J. Yuan, Y. Zhang, L. Zhou, G. Zhang, H.-L. Yip, T.-K. Lau, X. Lu, C. Zhu, H. Peng, P.A. Johnson, M. Leclerc, Y. Cao, J. Ulanski, Y. Li, Y. Zou, Single-junction organic solar cell with over 15% efficiency using fused-ring acceptor with electron-deficient core, Joule 3 (2019) 1140–1151, https://doi.org/10.1016/j.joule.2019.01.004.

[9] P. Apostol, J. Eccher, M.E.R. Dotto, C.B. Costa, T. Cazati, E.A. Hillard, H. Bock, I.H. Bechtold, High rectification in organic diodes based on liquid crystalline phthalocyanines, Phys. Chem. Chem. Phys. 17 (2015) 32390–32397, https://doi.org/10.1039/C5CP05582B.

[10] J. Eccher, A.C.B. Almeida, T. Cazati, H. von Seggern, H. Bock, I.H. Bechtold, Triplet exciplex electroluminescence from two columnar liquid crystal perylene derivatives, J. Lumin. 180 (2016) 31–37, https://doi.org/10.1016/j.jlumin.2016.08.012.

[11] T. Wöhrle, I. Wurzbach, J. Kirres, A. Kostidou, N. Kapernaum, J. Litterscheidt, J.C. Haenle, P. Staffeld, A. Baro, F. Giesselmann, S. Laschat, Discotic liquid crystals, Chem. Rev. 116 (2016) 1139–1241, https://doi.org/10.1021/acs.chemrev.5b00190.

[12] M. Kumar, S. Kumar, Liquid crystals in photovoltaics: a new generation of organic photovoltaics, Polym. J. 49 (2017) 85–111, https://doi.org/10.1038/pj.2016.109.

[13] M. Ozaki, M. Yoneya, Y. Shimizu, A. Fujii, Carrier transport and device applications of the organic semiconductor based on liquid crystalline non-peripheral octaalkyl phthalocyanine, Liq. Cryst. 45 (2018) 2376–2389, https://doi.org/10.1080/02678292.2018.1530375.

[14] T. Hori, T. Masuda, N. Fukuoka, T. Hayashi, Y. Miyake, T. Kamikado, H. Yoshida, A. Fujii, Y. Shimizu, M. Ozaki, Non-peripheral octahexylphthalocyanine doping effects in bulk heterojunction polymer solar cells, Org. Electron. 13 (2012) 335–340, https://doi.org/10.1016/j.orgel.2011.11.029.

[15] K. Petritsch, R.H. Friend, A. Lux, G. Rozenberg, S.C. Moratti, A.B. Holmes, Liquid crystalline phthalocyanines in organic solar cells, Synth. Met. 102 (1999) 1776–1777, https://doi.org/10.1016/S0379-6779(98)01035-2.

[16] M. Zhang, F. Zhang, Q. An, Q. Sun, W. Wang, X. Ma, J. Zhang, W. Tang, Nematic liquid crystal materials as a morphology regulator for ternary small molecule solar cells with power conversion efficiency exceeding 10%, J. Mater. Chem. A 5 (2017) 3589–3598, https://doi.org/10.1039/C7TA00211D.

[17] J. Eccher, W. Zajaczkowski, G.C. Faria, H. Bock, H. von Seggern, W. Pisula, I.H. Bechtold, Thermal evaporation versus spin-coating: electrical performance in columnar liquid crystal OLEDs, ACS Appl. Mater. Interfaces 7 (2015) 16374–16381, https://doi.org/10.1021/acsami.5b03496.

[18] S. Setia, S. Sidiq, J. De, I. Pani, S.K. Pal, Applications of liquid crystals in biosensing and organic light-emitting devices: future aspects, Liq. Cryst. 43 (2016) 2009–2050, https://doi.org/10.1080/02678292.2016.1213002.

[19] E.B. Melo, J. Eccher, P. Apostol, H. Bock, I.H. Bechtold, Characterization of liquid crystalline phthalocyanines for OFET applications, Mol. Cryst. Liq. Cryst. 657 (2017) 81–88, https://doi.org/10.1080/15421406.2017.1403232.

[20] N.B. Chaure, C. Pal, S. Barard, T. Kreouzis, A.K. Ray, A.N. Cammidge, I. Chambrier, M.J. Cook, C.E. Murphy, M.G. Cain, A liquid crystalline copper phthalocyanine derivative for high performance organic thin film transistors, J. Mater. Chem. 22 (2012) 19179, https://doi.org/10.1039/c2jm33301e.

[21] H.K. Bisoyi, Q. Li, Stimuli directed alignment of self-organized one-dimensional semiconducting columnar liquid crystal nanostructures for organic electronics, Prog. Mater. Sci. 104 (2019) 1–52, https://doi.org/10.1016/j.pmatsci.2019.03.005.

[22] M. Bajpai, N. Yadav, S. Kumar, R. Srivastava, R. Dhar, Incorporation of liquid crystalline triphenylene derivative in bulk heterojunction solar cell with molybdenum oxide as buffer layer for improved efficiency, Liq. Cryst. 43 (2016) 928–936, https://doi.org/10.1080/02678292.2016.1149239.

[23] P. Apostol, A. Bentaleb, M. Rajaoarivelo, R. Clérac, H. Bock, Regiospecific synthesis of tetrasubstituted phthalocyanines and their liquid crystalline order, Dalton Trans. 44 (2015) 5569–5576, https://doi.org/10.1039/C5DT00076A.

[24] M.M. Stylianakis, D. Konios, G. Viskadouros, D. Vernardou, N. Katsarakis, E. Koudoumas, S.H. Anastasiadis, E. Stratakis, E. Kymakis, Ternary organic solar cells incorporating zinc phthalocyanine with improved performance exceeding 8.5%, Dyes Pigm. 146 (2017) 408–413, https://doi.org/10.1016/j.dyepig.2017.07.032.

[25] T. Hori, N. Fukuoka, T. Masuda, Y. Miyake, H. Yoshida, A. Fujii, Y. Shimizu, M. Ozaki, Bulk heterojunction organic solar cells utilizing 1,4,8,11,15,18,22,25-octahexylphthalocyanine, Sol. Energy Mater. Sol. Cells (95,2011, 3087-3092), https://doi.org/10.1016/j.solmat.2011.06.039.

[26] C.J. Brabec, Organic photovoltaics: technology and market, Sol. Energy Mater. Sol. Cells 83 (2004) 273–292, https://doi.org/10.1016/j.solmat.2004.02.030.

[27] H. Wang, X. Wang, P. Fan, X. Yang, J. Yu, Enhanced power conversion efficiency of P3HT: PC 71 BM bulk heterojunction polymer solar cells by doping a high-mobility small organic molecule, Int. J. Photoenergy 2015 (2015) 1–8, https://doi.org/10.1155/2015/982064.

[28] K. Rahimi, I. Botiz, J.O. Agumba, S. Motamen, N. Stingelin, G. Reiter, Light absorption of poly(3-hexylthiophene) single crystals, RSC Adv. 4 (2014) 11121–11123, https://doi.org/10.1039/C3RA47064D.

[29] M.T. Dang, L. Hirsch, G. Wantz, P3HT:PCBM, best seller in polymer photovoltaic research, Adv. Mater. 23 (2011) 3597–3602, https://doi.org/10.1002/adma.201100792.

[30] S. Xing, H. Wang, Y. Zheng, J. Yu, Förster resonance energy transfer and energy cascade with a favorable small molecule in ternary polymer solar cells, Sol. Energy 139 (2016) 221–227, https://doi.org/10.1016/j.solener.2016.09.049.

[31] D. Devisscher, G. Reekmans, J. Kesters, P. Verstappen, J. Benduhn, N. Van den Brande, L. Lutsen, J. Manca, D. Vanderzande, K. Vandewal, P. Adriaensens, W. Maes, Analysis of bulk heterojunction organic solar cell blends by solid-state NMR relaxometry and sensitive external quantum efficiency – impact of polymer side chain variation on nanoscale morphology, Org. Electron. 74 (2019) 309–314, https://doi.org/10.1016/j.orgel.2019.06.046.

[32] W.C. Tsoi, D.T. James, J.S. Kim, P.G. Nicholson, C.E. Murphy, D.D.C. Bradley, J. Nelson, J.-S. Kim, The nature of in-plane skeleton Raman modes of P3HT and their correlation to the degree of molecular order in P3HT:PCBM blend thin films, J. Am. Chem. Soc. 133 (2011) 9834–9843, https://doi.org/10.1021/ja2013104.

[33] C.F.N. Marchiori, Y. Garcia-Basabe, F. de A. Ribeiro, M. Koehler, L.S. Roman, M.L.M. Rocco, Thermally induced anchoring of fullerene in copolymers with Si-bridging atom: spectroscopic evidences, Spectrochim. Acta Part A Mol. Biomol. Spectrosc. 171 (2017) 376–382, https://doi.org/10.1016/j.saa.2016.08.010.

[34] J.F.P. Souza, J.P.M. Serbena, E.L. Kowalski, L.C. Akcelrud, Determination of P3HT trap site energies by thermally stimulated current, J. Electron. Mater. 47 (2018) 1611–1619, https://doi.org/10.1007/s11664-017-5965-z.

[35] J. Eccher, G.C. Faria, H. Bock, H. von Seggern, I.H. Bechtold, Order induced charge carrier mobility enhancement in columnar liquid crystal diodes, ACS Appl. Mater. Interfaces 5 (2013) 11935–11943, https://doi.org/10.1021/am403681q.

[36] H. Derouiche, H. Ben Miled, A.B. Mohamed, Enhanced performance of a CuPc: PCBM based solar cell using bathocuproine BCP or nanostructured TiO2 as hole-blocking layer, Phys. Status Solidi 207 (2010) 479–483, https://doi.org/10.1002/pssa.200925424.

[37] B.Y. Kadem, M.K. Al-hashimi, A.K. Hassan, The effect of solution processing on the power conversion efficiency of P3HT-based organic solar cells, Energy Procedia 50 (2014) 237–245, https://doi.org/10.1016/j.egypro.2014.06.029.

[38] W. Gao, T. Liu, R. Ming, Z. Luo, K. Wu, L. Zhang, J. Xin, D. Xie, G. Zhang, W. Ma, H. Yan, C. Yang, Near-infrared small molecule acceptor enabled high-performance nonfullerene polymer solar cells with over 13% efficiency, Adv. Funct. Mater. 28 (2018) 1803128, , https://doi.org/10.1002/adfm.201803128.

[39] H. Bässler, Charge transport in disordered organic photoconductors a Monte Carlo simulation study, Phys. Status Solidi 175 (1993) 15–56, https://doi.org/10.1002/pssb.2221750102.

[40] M. Park, F. Kim, Synergistic effects of processing additives and thermal annealing on nanomorphology and hole mobility of poly(3-hexylthiophene) thin films, Polymers (Basel) 11 (2019) 112, https://doi.org/10.3390/polym11010112.

[41] F. Laquai, D. Andrienko, R. Mauer, P.W.M. Blom, Charge carrier transport and photogeneration in P3HT:PCBM photovoltaic blends, Macromol. Rapid Commun. 36 (2015) 1001–1025, https://doi.org/10.1002/marc.201500047.